



## BRIEF REPORT

10.1002/2014JA019939

## Key Points:

- Chorus wave distributions as a function of  $A_e$  and solar wind parameters
- Chorus waves and acceleration and loss of radiation belt electrons
- Upper band and lower band chorus wave emission

## Correspondence to:

H. Aryan,  
 aryan.homayon@gmail.com

## Citation:

Aryan, H., K. Yearby, M. Balikhin, O. Agapitov, V. Krasnoselskikh, and R. Boynton (2014), Statistical study of chorus wave distributions in the inner magnetosphere using  $A_e$  and solar wind parameters, *J. Geophys. Res. Space Physics*, 119, 6131–6144, doi:10.1002/2014JA019939.

Received 3 MAR 2014

Accepted 23 JUL 2014

Accepted article online 28 JUL 2014

Published online 18 AUG 2014

## Statistical study of chorus wave distributions in the inner magnetosphere using $A_e$ and solar wind parameters

Homayon Aryan<sup>1</sup>, Keith Yearby<sup>1</sup>, Michael Balikhin<sup>1</sup>, Oleksiy Agapitov<sup>2,3</sup>, Vladimir Krasnoselskikh<sup>4</sup>, and Richard Boynton<sup>1</sup>

<sup>1</sup>Department of Automatic Control and Systems Engineering, University of Sheffield, Sheffield, UK, <sup>2</sup>Space Sciences Laboratory, University of California, Berkeley, California, USA, <sup>3</sup>Astronomy and Space Physics Department, Taras Shevchenko National, University of Kiev, Kiev, Ukraine, <sup>4</sup>LC2E/CNRS, University of Orléans, Orleans, France

**Abstract** Energetic electrons within the Earth's radiation belts represent a serious hazard to geostationary satellites. The interactions of electrons with chorus waves play an important role in both the acceleration and loss of radiation belt electrons. The common approach is to present model wave distributions in the inner magnetosphere under different values of geomagnetic activity as expressed by the geomagnetic indices. However, it has been shown that only around 50% of geomagnetic storms increase flux of relativistic electrons at geostationary orbit while 20% causes a decrease and the remaining 30% has relatively no effect. This emphasizes the importance of including solar wind parameters such as bulk velocity ( $V$ ), density ( $n$ ), flow pressure ( $P$ ), and the vertical interplanetary magnetic field component ( $B_z$ ) that are known to be predominately effective in the control of high energy fluxes at the geostationary orbit. Therefore, in the present study the set of parameters of the wave distributions is expanded to include the solar wind parameters in addition to the geomagnetic activity. The present study examines almost 4 years (1 January 2004 to 29 September 2007) of Spatio-Temporal Analysis of Field Fluctuation data from Double Star TC1 combined with geomagnetic indices and solar wind parameters from OMNI database in order to present a comprehensive model of wave magnetic field intensities for the chorus waves as a function of magnetic local time, L shell ( $L$ ), magnetic latitude ( $\lambda_m$ ), geomagnetic activity, and solar wind parameters. Generally, the results indicate that the intensity of chorus emission is not only dependent upon geomagnetic activity but also dependent on solar wind parameters with velocity and southward interplanetary magnetic field  $B_s$  ( $B_z < 0$ ), evidently the most influential solar wind parameters. The largest peak chorus intensities in the order of 50 pT are observed during active conditions, high solar wind velocities, low solar wind densities, high pressures, and high  $B_s$ . The average chorus intensities are more extensive and stronger for lower band chorus than the corresponding upper band chorus.

### 1. Introduction

Energetic electrons in the space environment represent a serious hazard to geostationary satellites that are increasingly used for communication, navigation, Earth observation, and defense. The impact of such relativistic electrons on satellites can range from single event upsets, which are followed by full recovery, to permanent failure of individual subsystems, or even complete loss of the satellite [Blake et al., 1992; Fennell et al., 2001]. Energetic electrons are mainly trapped within the Earth's inner ( $1.1 < L < 2$ ) and outer ( $3 < L < 7$ ) radiation belts which are separated by what is known as the slot region. The inner radiation belt is relatively stable and only varies during intense geomagnetic storms [Li et al., 1999; Millan and Thorne, 2007]. However, the outer radiation belt is highly dynamic and the flux of energetic electrons can vary by several orders of magnitude during geomagnetic storms and other disturbances [Craven, 1966; Blake et al., 1992; Baker et al., 1994; Reeves et al., 2003; Baker and Kanekal, 2008; Tu et al., 2009]. The interaction of gyroresonant particles with chorus waves largely determines the dynamics of the Earth's radiation belts [Meredith et al., 2002; Thorne et al., 2005; Xiao et al., 2009, 2010] that affects the acceleration and loss of radiation belt electrons [Bortnik and Thorne, 2007; Li et al., 2007; Shprits et al., 2009; Artemyev et al., 2013; Thorne et al., 2013; Baker et al., 2014]. Meanwhile, the slot region between the inner and the outer radiation belt is widely accepted to have formed as a result of energetic electron loss due to pitch angle scattering by very low frequency waves such as plasmaspheric hiss [Lyons et al., 1972] and magnetosonic waves [Mourenas et al., 2013]. Evidence points to whistler mode chorus as the main source of plasmaspheric hiss [Bortnik et al.,

This is an open access article under the terms of the Creative Commons Attribution License, which permits use, distribution and reproduction in any medium, provided the original work is properly cited.

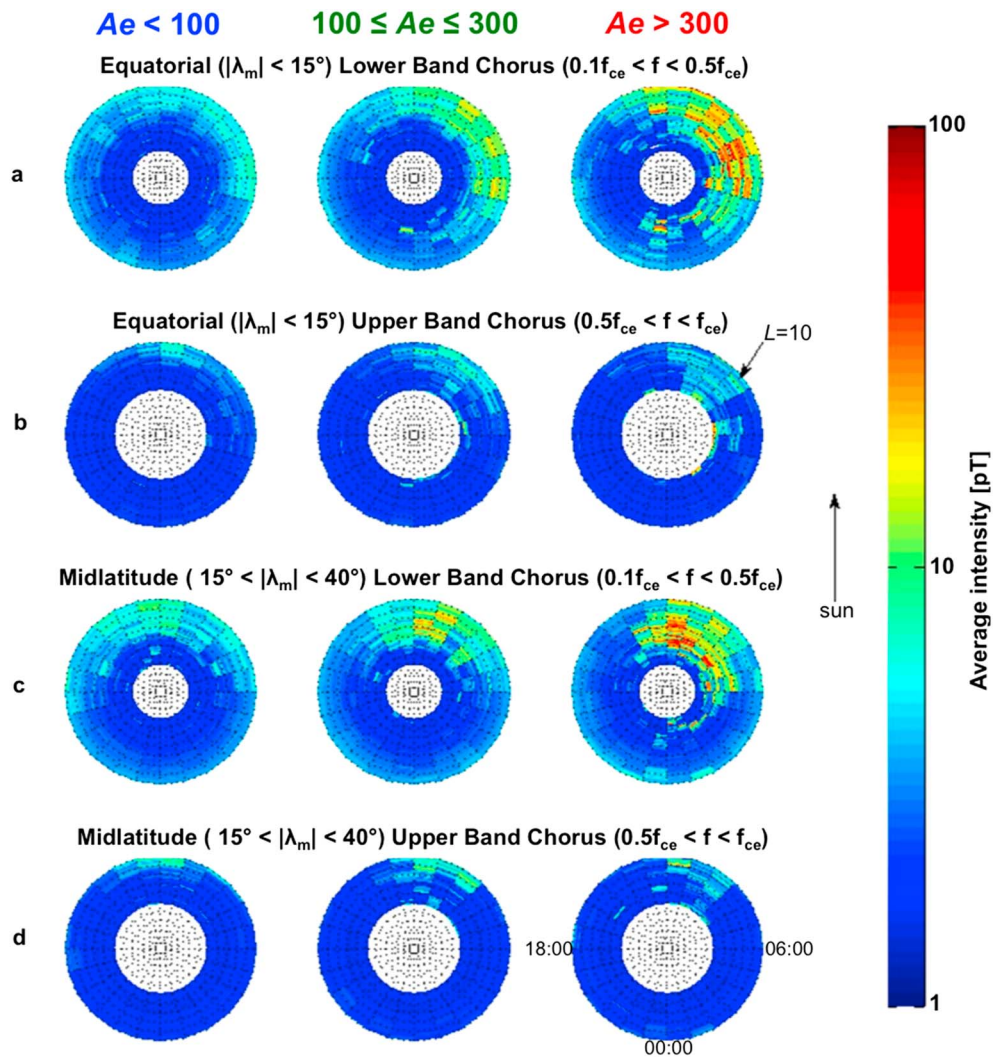


**Figure 1.** The (a) equatorial ( $|\lambda_m| < 15^\circ$ ) lower band, (b) equatorial upper band, (c) midlatitude ( $15^\circ \leq |\lambda_m| \leq 40^\circ$ ) lower band, and (d) midlatitude upper band average chorus intensities as a function of  $L$ , MLT, and geomagnetic activity during (left column) quiet, (middle column) moderate, and (right column) active conditions.

2009] which is also accountable for the decay of energetic electrons in the outer radiation belt during relatively quiet times [Summers *et al.*, 2007].

Chorus emissions are very intense right-hand polarized electromagnetic whistler mode waves that are excited naturally in the low-density region near the geomagnetic equator outside the plasmopause [Burtis and Helliwell, 1969; LeDocq *et al.*, 1998; Lauben *et al.*, 2002; Santolik *et al.*, 2005; Li *et al.*, 2011], and they are observed in two separate frequency bands: the lower band ( $0.1f_{ce} < f < 0.5f_{ce}$ ) and the upper band ( $0.5f_{ce} < f < f_{ce}$ ) [Helliwell, 1967; Tsurutani and Smith, 1974; Agapitov *et al.*, 2013] where  $f_{ce}$  is the electron cyclotron frequency. The common approach is to present model wave distributions in the inner magnetosphere under different values of geomagnetic activity as expressed by the geomagnetic indices ( $Kp$  and  $Ae$ ) [Li *et al.*, 2011; Meredith *et al.*, 2012; Agapitov *et al.*, 2012, 2013]. It has been shown that chorus wave emission is dependent on geomagnetic activity with peak intensities observed during active conditions. Meredith *et al.* [2012] concluded that the largest chorus wave intensities were observed with equatorial lower band chorus between 2300 and 1200 magnetic local time (MLT). However, Reeves *et al.* [2003] examined 276 geomagnetic storms of which only 53% increased, 19% decreased, and the remaining 28% left the flux of relativistic electrons in the radiation belt relatively unchanged. This indicates the importance of expanding the set of parameters of the wave distributions to include solar wind parameters as well as geomagnetic indices. It is known that solar wind parameters are predominately effective in the control of energetic

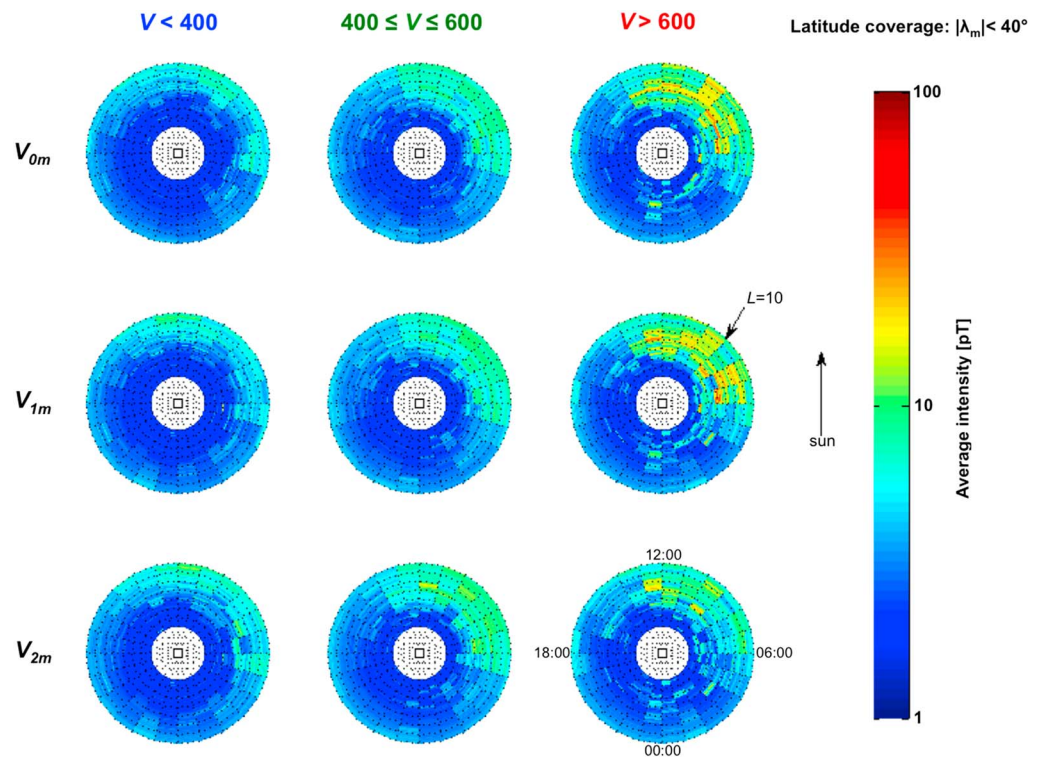


**Figure 2.** Average chorus intensities as a function of  $L$ , MLT, and  $V$  for (left column) slow, (middle column) moderate, and (right column) fast solar wind velocities. Results are shown for maximum solar wind velocity observed on (top row) current day ( $V_{0m}$ ), (middle row) previous day ( $V_{1m}$ ), and (bottom row) 2 days ago ( $V_{2m}$ ).

electron fluxes at the geostationary orbit [Onsager et al., 2007; Ohtani et al., 2009; Balikhin et al., 2011; Matsumura et al., 2011; Reeves et al., 2011, 2013]. Recently, Boynton et al. [2013] applied the NARMAX (Nonlinear Autoregressive Moving Average modelling) algorithm [Balikhin et al., 2010, 2011] to show the importance of solar wind parameters that control the flux of energetic electrons at geostationary orbit and identified solar wind velocity as the most influential parameter. Therefore, in the present study the set of parameters of the wave distributions are expanded to include solar wind parameters, such as bulk velocity, density, flow pressure, and the vertical interplanetary magnetic field component ( $B_z$ ), in addition to geomagnetic activity. This study analyzes almost 4 years (1 January 2004 to 29 September 2007) of Double Star TC1 Spatio-Temporal Analysis of Field Fluctuation (STAFF) and OMNI data in order to present the wave magnetic field intensities for the lower and upper band chorus waves as a function of MLT,  $\lambda_m$ ,  $L$ , geomagnetic index ( $A_e$ ), and solar wind parameters (velocity,  $V$ , density,  $n$ , pressure,  $P$ , and the vertical interplanetary magnetic field component ( $B_z$ )).

## 2. Description of the Data Set

Double Star was launched on 29 December 2003 as a joint mission by the European Space Agency, ESA, and China National Space Administration. The equatorial satellite, TC1, operates in an elliptical orbit with a perigee of 562 km and an apogee of 78,970 km. The STAFF (Spatio-Temporal Analysis of Field Fluctuation) experiment on board TC1 computes the spectral matrix at 27 different frequencies (between 10 Hz and 4 kHz) with a 1 s resolution using a Digital Wave Processor (DWP) [Cornilleau-Wehrin et al., 2005] provided by the University of Sheffield. At these frequencies, where the available telemetry does not permit acquisition of the waveform, spectrum analysis is performed onboard. After the data pass through an antialias filter, DWP digitizes the three components of the waveform at a 10 kHz sampling rate. A complex fast Fourier transform (FFT) is then calculated and processed to get a spectral matrix in 27 roughly logarithmically spaced channels (similar to that of Cluster). The spectrum analyzer data are then processed on the ground to minimize the interference resulting from the nondeployment of

**Table 1.** The Kullback-Leibler Distance ( $D_{KL}$ ) Between Slow and Moderate ( $D_{KLsm}$ ), Slow and Fast ( $D_{KLsf}$ ), and Moderate and Fast ( $D_{KLmf}$ ) Solar Wind Velocities for  $V_{0m}$ ,  $V_{1m}$ , and  $V_{2m}$  as Presented in Figure 2

	$D_{KLsm}$	$D_{KLmf}$	$D_{KLsf}$
$V_{0m}$	0.0270	0.0395	0.0534
$V_{1m}$	0.0258	0.0513	0.0635
$V_{2m}$	0.0298	0.0448	0.0458

the antenna boom. This is done by rejecting spectra acquired when large interference spikes occur and by combining the signals from two axes of the antenna to synthesize a measurement in a direction where continuous interference is least. The optimum direction is adjusted as a function of frequency and spin phase. This study analyzes almost 4 years (1 January 2004 to 29 September 2007) of Double Star TC1 STAFF and OMNI data. The geomagnetic index ( $A_e$ ) and the solar wind parameters ( $V$ ,  $n$ , and  $P$ ) used are 1 h values available online at OMNI database. The vertical interplanetary magnetic field component ( $B_z$ ) used are 1 min values that are also available online at OMNI database. The  $L$  parameter is binned in linear steps of  $0.2L$ , and the MLT parameter is binned in linear steps of 1 h of MLT. The lower and upper band chorus wave intensities are calculated over the frequency ranges ( $0.1f_{ce} < f < 0.5f_{ce}$ ) and ( $0.5f_{ce} < f < f_{ce}$ ), respectively. The data are only selected in the cases where all of a given frequency band fall within the frequency range; otherwise, the data are rejected. All data are in SI units ( $A_e$  (nT),  $V$  (km/s),  $n$  (n/cc),  $P$  (nPa), and  $B_z$  (nT)).

### 3. Results

#### 3.1. Average Chorus Intensities as a Function of Geomagnetic Activity

The distributions of chorus wave in the inner magnetosphere can be presented under different values of geomagnetic activity as expressed by the geomagnetic indices. Figure 1 shows the equatorial ( $|\lambda_m| < 15^\circ$ ) lower band (a), equatorial upper band (b), midlatitude ( $15^\circ \leq |\lambda_m| \leq 40^\circ$ ) lower band (c), and midlatitude upper band (d) average chorus intensities as a function of  $L$ , MLT, and geomagnetic activity during quiet (left), moderate (middle), and active (right) conditions. Results show that both the equatorial (Figure 1b) and midlatitude (Figure 1d) upper band chorus intensities are relatively weak even during active conditions with peak values largely below 10 pT. The peak chorus intensities are mostly confined in the regions from 0500 to 1300 MLT (equatorial) and from 0900 to 1400 MLT (midlatitude) and marginally intensify with increasing geomagnetic activity. On the other hand, the lower band chorus intensities (Figures 1a and 1c) are far more extensive and stronger than the corresponding upper band chorus. The peak lower band chorus intensities rise to 10 pT and 20 pT, primarily from premidnight to the afternoon sector, during quiet and moderate conditions, respectively. The largest intensities of the order 50 pT are observed for lower band chorus during active conditions in the region of  $4 \leq L \leq 9$  from 2300 to 1300 MLT (equatorial) and from 0500 to 1400 MLT (midlatitude). By large, the peak intensities of the midlatitude chorus are similar in magnitude to the corresponding equatorial chorus intensities. However, the peak intensities for midlatitude region predominantly occur within a smaller MLT sector than the corresponding equatorial chorus intensities. For example, the peak intensities of midlatitude lower band chorus during active conditions mainly occur from 0500 to 1400 MLT compared to a more extensive spread from 2300 to 1300 MLT seen for equatorial lower band chorus. The results are largely consistent with previous studies that presented model wave distributions in the inner magnetosphere under different values of geomagnetic activity as expressed by the geomagnetic indices [Meredith *et al.*, 2003; Li *et al.*, 2011; Meredith *et al.*, 2012; Agapitov *et al.*, 2012, 2013]. In particular, the results here agree with the results of Meredith *et al.* [2012] who presented a combined satellite (DE1 (3 years), CRRES (15 months), Cluster 1 (10 years), Double Star TC1 (1 year), and THEMIS (17 months)) model of the equatorial and midlatitude wave intensity for the upper and lower band chorus also as a function of  $A_e$ .

#### 3.2. Average Chorus Intensities as a Function of Solar Wind Parameters

As mentioned earlier, Reeves *et al.* [2003] concluded that only 53% of geomagnetic storms increase the flux of relativistic electrons at geostationary orbit while 19% cause a decrease and the remaining 28 have no significant effect. This emphasizes the importance of including solar wind parameters in addition to geomagnetic indices in order to better understand the distributions of chorus wave in the magnetosphere. The following sections reveal the average chorus intensities as a function of solar wind velocity, density, pressure, and interplanetary magnetic field,  $B_z$ , respectively.

##### 3.2.1. Average Chorus Intensities as a Function of Velocity

Solar wind parameters are known to be predominately effective in the control of high energy fluxes at geostationary orbit with solar wind velocity considered as the most influential parameter [Boynnton *et al.*, 2013]. Figure 2 shows the average lower band chorus intensities as a function of  $L$ , MLT, and  $V$  for slow (left

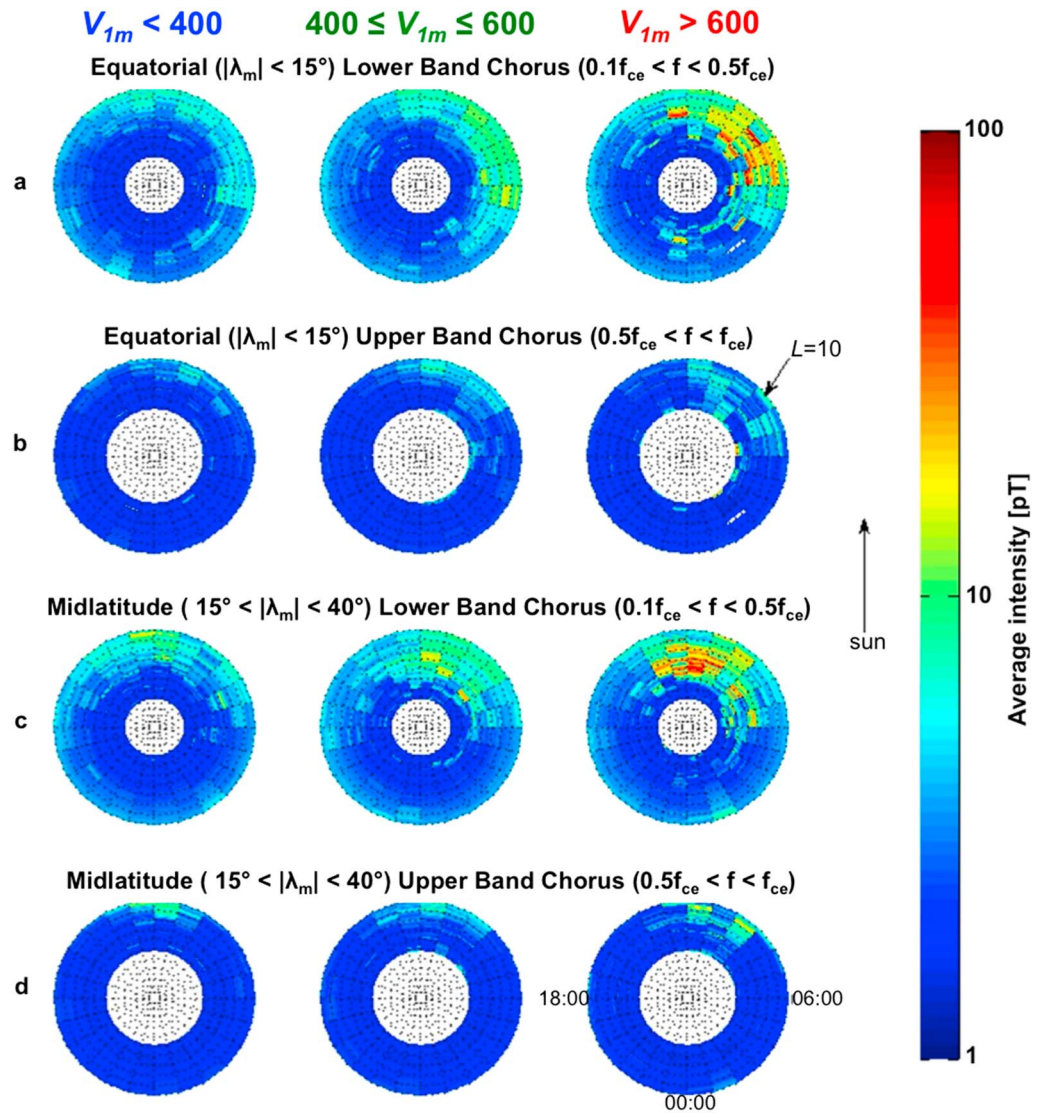


**Figure 3.** The (a) equatorial ( $|\lambda_m| < 15^\circ$ ) lower band, (b) equatorial upper band, (c) midlatitude ( $15^\circ \leq |\lambda_m| \leq 40^\circ$ ) lower band, and (d) midlatitude upper band average chorus intensities as a function of  $L$ , MLT, and maximum solar wind velocity from previous day ( $V_{1m}$ ) for (left column) slow, (middle column) moderate, and (right column) fast solar wind velocities.

column), moderate (middle column), and fast (right column) solar wind velocities. It is commonly accepted that temporal changes in solar wind parameters are not immediately observed at the geostationary orbit. In fact, there is a time delay of approximately 1–2 days depending on the energy [Paulikas and Blake, 1979; Li et al., 2005; Boynton et al., 2011; Reeves et al., 2011; Aryan et al., 2013]. The interplay between the local acceleration and outward/inward radial diffusion mainly determines the time delay. While chorus emissions are generated over a wider range, a similar time delay may still apply. Consequently, Figure 2 includes maximum solar wind velocity from current day ( $V_{0m}$ , top row), 1 day ( $V_{1m}$ , middle row), and 2 days ( $V_{2m}$ , bottom row) ago (the subscript,  $*$   $m$ , represents maximum value, and the corresponding number indicates days delay). Results show that the average chorus intensities as a function of solar wind velocity follows a noticeably similar trend to that of chorus intensities as a function of geomagnetic activity. In this case, the average chorus intensities rise with increasing solar wind velocity in all three cases of delay. However, it is not immediately clear which of the three cases of delay provides the most widespread statistical distribution. Therefore, the Kullback-Leibler [Kullback and Leibler, 1951; Kullback, 1959] theory was applied in order to identify the case with the most widespread statistical distribution. The Kullback-Leibler theory calculates the difference

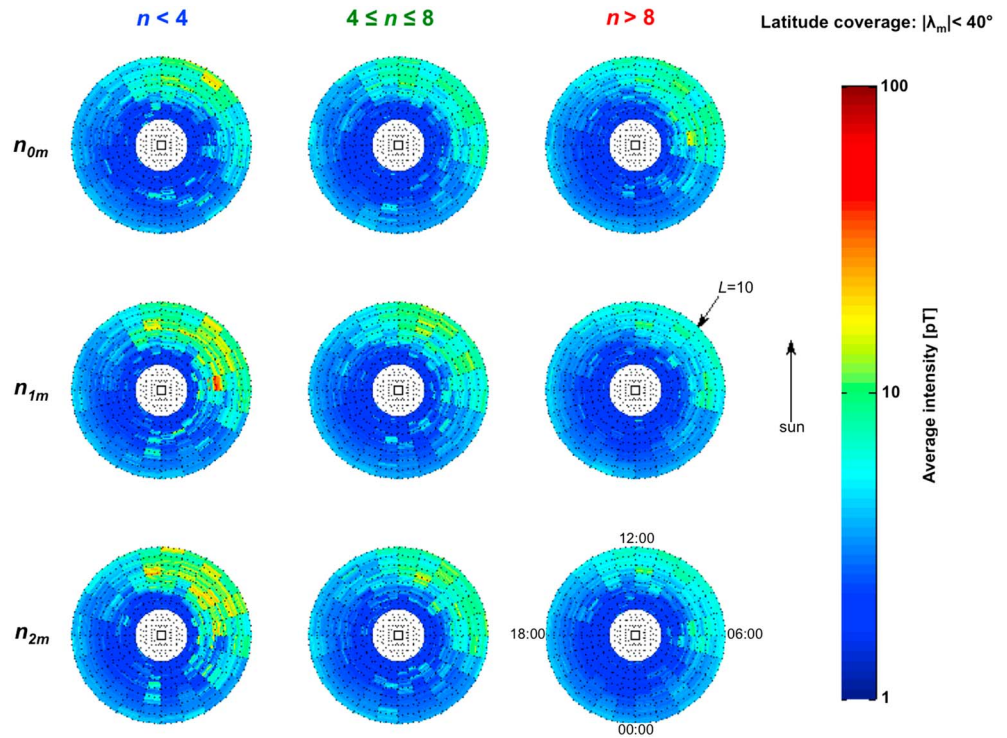


**Figure 4.** Average chorus intensities as a function of  $L$ , MLT, and  $n$  for (left column) low, (middle column) moderate, and (right column) high solar wind densities. Results are shown for maximum solar wind density observed on (top row) current day ( $n_{0m}$ ), (middle row) previous day ( $n_{1m}$ ), and (bottom row) 2 days ago ( $n_{2m}$ ).

between two probability distributions (e.g.,  $X$  and  $Y$ ) given as a number known as the Kullback-Leibler Distance ( $D_{KL}$ ) which is essentially the distance of  $X$  from  $Y$ , with  $X$  and  $Y$  normalized, defined by equation (1).

$$D_{KL} = \sum_i X_i \cdot \log_2(X_i/Y_i) \quad (1)$$

A  $D_{KL}$  value of zero implies that the two probability distributions are identical. The Kullback-Leibler theory was applied to the results in Figure 2 in the following way: first, calculate  $D_{KL}$  between slow and moderate ( $D_{KLsm}$ ), slow and fast ( $D_{KLsf}$ ), and moderate and fast ( $D_{KLmf}$ ) solar wind velocities for each particular cases of delay; then verify the validity of the distribution for each cases of delay (a distribution is only valid if  $D_{KLsf} > D_{KLsm}$  and  $D_{KLsf} > D_{KLmf}$  i.e., the largest difference is expected between the two extreme distributions; in this case between slow and fast solar wind velocities); finally, the distribution with the highest value of  $D_{KLsf}$  amongst the valid distributions is selected (larger values of  $D_{KL}$  suggests broader distribution). The values of  $D_{KLsm}$ ,  $D_{KLsf}$ ,  $D_{KLmf}$  for  $V_{0m}$ ,  $V_{1m}$ , and  $V_{2m}$  are presented in Table 1. The results show that all three cases of delay provide valid distributions. However, the most widespread statistical distribution is observed with maximum solar wind velocity from previous day ( $V_{1m}$ ) with the largest  $D_{KLsf}$  value of 0.0635.

**Table 2.** The Kullback-Leibler Distance ( $D_{KL}$ ) Between Low and Moderate ( $D_{KLlm}$ ), Low and High ( $D_{KLlh}$ ), and Moderate and High ( $D_{KLmh}$ ) Solar Wind Densities for  $n_{0m}$ ,  $n_{1m}$ , and  $n_{2m}$  as Presented in Figure 4

	$D_{KLlm}$	$D_{KLmh}$	$D_{KLlh}$
$n_{0m}$	0.0368	0.0307	0.0412
$n_{1m}$	0.0447	0.0305	0.0500
$n_{2m}$	0.0583	0.0293	0.0580

Figure 3 shows the equatorial ( $|\lambda_m| < 15^\circ$ ) lower band (a), equatorial upper band (b), midlatitude ( $15^\circ \leq |\lambda_m| \leq 40^\circ$ ) lower band (c), and midlatitude upper band (d) average chorus intensities as a function of  $L$ , MLT, and maximum solar wind velocity from previous day ( $V_{1m}$ ) for slow (left column), moderate (middle column), and fast (right column) solar wind velocities. The results show significant similarities to the corresponding average equatorial and midlatitude lower and upper band chorus intensities as a function of geomagnetic activity seen in Figure 1. The upper band chorus intensities are generally weak with peak values of less than 10 pT even during active conditions. The peak

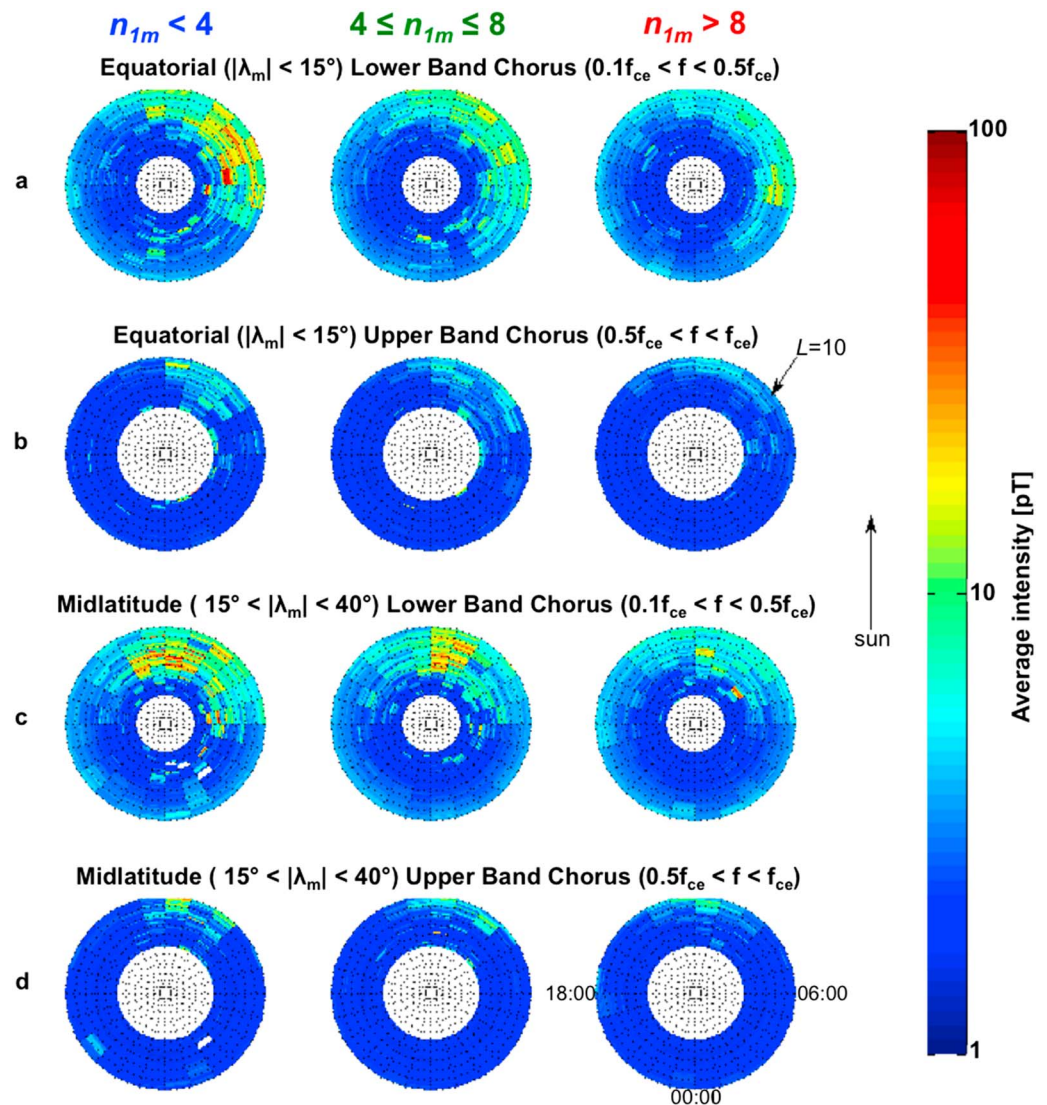


**Figure 5.** The (a) equatorial ( $|\lambda_m| < 15^\circ$ ) lower band, (b) equatorial upper band, (c) midlatitude ( $15^\circ \leq |\lambda_m| \leq 40^\circ$ ) lower band, and (d) midlatitude upper band average chorus intensities as a function of  $L$ , MLT, and maximum solar wind density from previous day ( $n_{1m}$ ) for (left column) low, (middle column) moderate, and (right column) high solar wind densities.

intensities largely occur within the regions of 0600 to 1200 MLT (equatorial) and 1000 to 1400 MLT (midlatitude) and rise slightly with increasing velocity. The lower band chorus is more extensive, occurring in the region  $4 \leq L \leq 9$  from 0300 to 1300 MLT (equatorial) and from 0300 to 1300 MLT (midlatitude), and stronger in compression to the corresponding upper band chorus with peak intensities rising to 15 pT, 20 pT, and 50 pT during slow, moderate, and fast solar wind velocities, respectively. The occurrence of peak lower band chorus intensities during active conditions (Figure 1) is slightly higher than during fast solar wind velocities (Figure 3). The peak intensities of midlatitude chorus are approximately equal in magnitude to the corresponding equatorial chorus intensities but mainly occur at smaller MLT sector. The results prove that there is a strong dependency between the intensity of chorus emission and solar wind velocity.

**3.2.2. Average Chorus Intensities as a Function of Density**

Another important solar wind parameter is density which is known to be influential in the control of high energy fluxes at geostationary orbit where it plays a crucial role in defining the relationship between energetic electron fluxes and solar wind velocity [Aryan *et al.*, 2013]. Figure 4 shows the average wave intensities as a function of  $L$ , MLT, and  $n$  for low (left column), moderate (middle column), and high (right column) solar wind densities. Once again, the time delay introduced by the magnetospheric system is considered, and

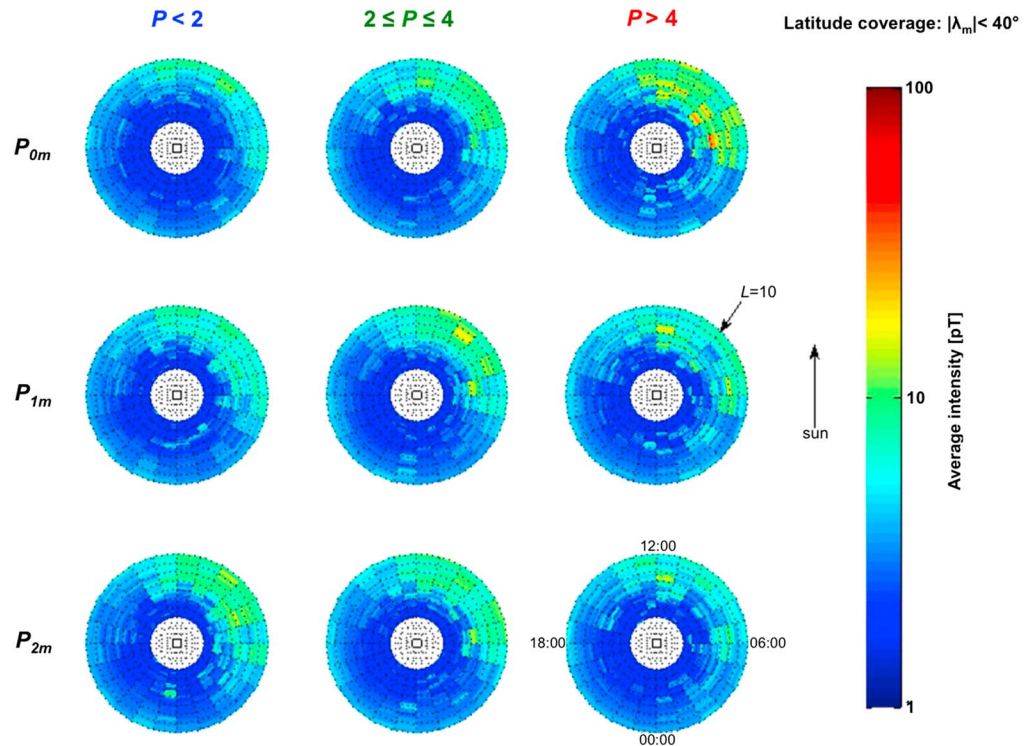


**Figure 6.** Average chorus intensities as a function of  $L$ , MLT, and  $P$  for (left column) low, (middle column) moderate, and (right column) high pressures. Results are shown for maximum pressure observed on (top row) current day ( $P_{0m}$ ), (middle row) previous day ( $P_{1m}$ ), and (bottom row) 2 days ago ( $P_{2m}$ ).

therefore, the average lower band chorus is shown for maximum density from the current day ( $n_{0m}$ , top row), previous day ( $n_{1m}$ , middle row), and 2 days ( $n_{2m}$ , bottom row) ago. In contrast to solar wind velocity (Figure 2), the average chorus intensities decline with increasing solar wind density. The Kullback-Leibler theory was applied to calculate  $D_{KL}$  between low and moderate ( $D_{KLlm}$ ), low and high ( $D_{KLlh}$ ), and moderate and high ( $D_{KLmh}$ ) solar wind densities for each particular cases of delay, as shown in Table 2. Here the distributions of  $n_{0m}$  (top row) and  $n_{1m}$  (middle row) are valid. However, the distribution of  $n_{2m}$  (bottom row) is invalid because  $D_{KLlm} > D_{KLlh}$ . Amongst the two valid distributions, the most widespread statistical distribution is observed with maximum solar wind density from previous day ( $n_{1m}$ ) with the largest  $D_{KLlh}$  value of 0.0500.

Figure 5 shows the equatorial ( $|\lambda_m| < 15^\circ$ ) lower band (a), equatorial upper band (b), midlatitude ( $15^\circ \leq |\lambda_m| \leq 40^\circ$ ) lower band (c), and midlatitude upper band (d) average chorus intensities as a function of  $L$ , MLT, and maximum solar wind density from previous day ( $n_{1m}$ ) for low (left column), moderate (middle column), and high (right column) solar wind densities. Again, the upper band chorus intensities are mostly weak with peak values of less than 10 pT. The peak intensities largely occur within the regions of 0600 to 1200 MLT (equatorial) and 1000 to 1400 MLT (midlatitude) and drop slightly with increasing density. The lower band chorus is more extensive, occurring in the region  $4 \leq L \leq 9$  from 0500 to 1100 MLT (equatorial) and from 0600 to 1400 MLT (midlatitude), and stronger in compression to the corresponding upper band chorus with peak intensities rising to 50 pT, 20 pT, and 15 pT during low, moderate, and high solar wind densities, respectively. However, the occurrence of peak lower band chorus intensities during low solar wind densities (Figure 5) is lower than during active conditions (Figure 1) and during fast solar wind velocities (Figure 3). By large, the peak intensities of midlatitude chorus are roughly equal in magnitude to the corresponding equatorial chorus intensities. In contrast, the peak intensities for midlatitude region predominantly occur within a smaller MLT sector than the corresponding equatorial chorus intensities, a similar

**Table 3.** The Kullback-Leibler Distance ( $D_{KL}$ ) Between Low and Moderate ( $D_{KLlm}$ ), Low and High ( $D_{KLlh}$ ), and Moderate and High ( $D_{KLmh}$ ) Pressures for  $P_{0m}$ ,  $P_{1m}$ , and  $P_{2m}$  as Presented in Figure 6

	$D_{KLlm}$	$D_{KLmh}$	$D_{KLlh}$
$P_{0m}$	0.0296	0.0426	0.0517
$P_{1m}$	0.0349	0.0429	0.0413
$P_{2m}$	0.0410	0.0327	0.0453

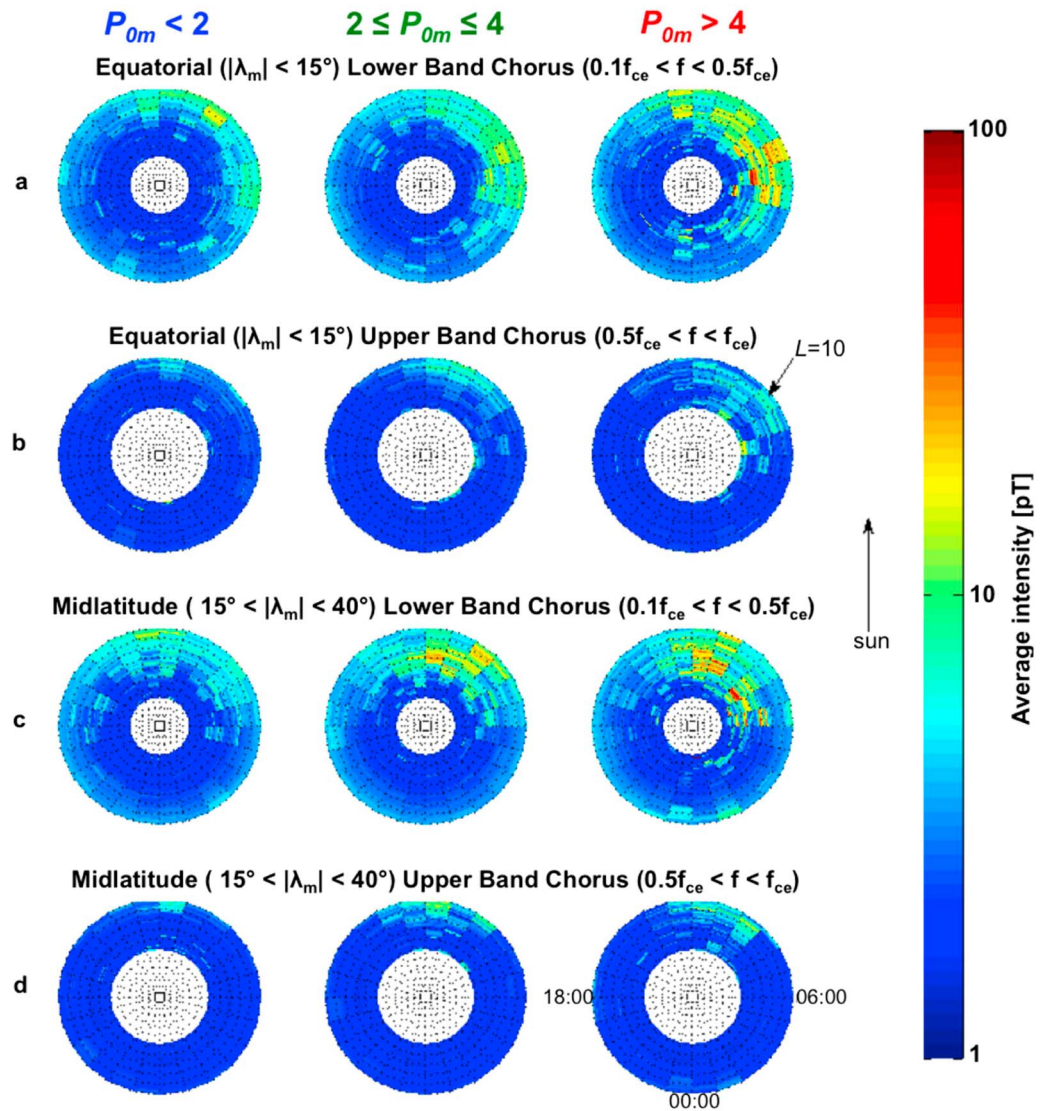


**Figure 7.** The (a) equatorial ( $|\lambda_m| < 15^\circ$ ) lower band, (b) equatorial upper band, (c) midlatitude ( $15^\circ \leq |\lambda_m| \leq 40^\circ$ ) lower band, and (d) midlatitude upper band average chorus intensities as a function of  $L$ , MLT, and maximum current day pressure ( $P_{0m}$ ) for (left column) low, (middle column) moderate, and (right column) high pressures.

trend to solar wind velocity and geomagnetic activity. Evidently, the results show convincing dependency between the intensity of chorus emission and solar wind density.

### 3.2.3. Average Chorus Intensities as a Function of Flow Pressure

Flow pressure is a function of velocity and density that is also known to contribute in the control of high energy fluxes at the geostationary orbit. Figure 6 presents the average lower band chorus intensities as a function of  $L$ , MLT, and  $P$  for low (left column), moderate (middle column), and high (right column) pressures. The results are shown for maximum pressure from the current day ( $P_{0m}$ , top row), previous day ( $P_{1m}$ , middle row), and 2 days ( $P_{2m}$ , bottom row) ago in order to take into account the time delay introduced by the magnetospheric system. Similar to solar wind velocity (Figure 1), the average chorus intensities rise with increasing pressure. The Kullback-Leibler theory was applied to calculate  $D_{KL}$  between low and moderate ( $D_{KLm}$ ), low and high ( $D_{KLh}$ ), and moderate and high ( $D_{KLmh}$ ) pressures for each particular cases of delay, shown in Table 3. In this case, the most widespread statistical distribution is observed with current day maximum pressure ( $P_{0m}$ , top row) with the largest  $D_{KLh}$  value of 0.0517.

Figure 7 shows the equatorial ( $|\lambda_m| < 15^\circ$ ) lower band (a), equatorial upper band (b), midlatitude ( $15^\circ \leq |\lambda_m| \leq 40^\circ$ ) lower band (c), and midlatitude upper band (d) average chorus intensities as a function

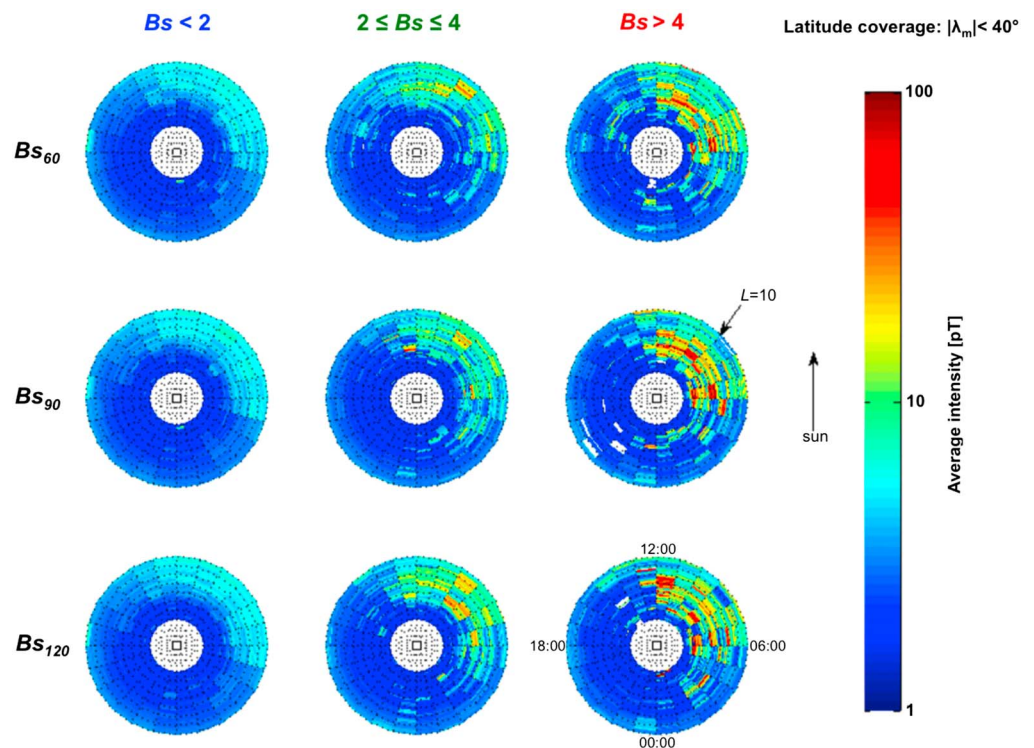


**Figure 8.** Average chorus intensities as a function of  $L$ , MLT, and  $B_s$  for (left column) low, (middle column) moderate, and (right column) high  $B_s$ . Results are shown for  $B_s$  with (top row) 60 ( $B_{s60}$ ), (middle row) 90 ( $B_{s90}$ ), and (bottom row) 120 ( $B_{s120}$ ) min of delay.

of  $L$ , MLT, and maximum current day pressure ( $P_{0m}$ ) for low (left column), moderate (middle column), and high (right column) pressures. The results show significant similarities to solar wind velocity (Figure 3) and geomagnetic activity (Figure 1) with regards to the intensities of chorus emission. Generally, the average chorus intensities rise with increasing pressure. The average lower band chorus intensities are larger than the corresponding upper band chorus intensities. However, the occurrence of peak lower band chorus intensities during high pressures (Figure 7) is slightly lower than during active conditions (Figure 1) and during fast solar wind velocities (Figure 3). The results prove that the intensity of chorus emission is also dependent upon pressure.

### 3.2.4. Average Chorus Intensities as a Function of Flow $B_z$

High energy flux enhancement depends not only on the solar wind velocity and density but also on the vertical interplanetary magnetic field component ( $B_z$ ). The southward interplanetary magnetic field ( $B_z < 0$ ) causes large flux enhancement due to strong coupling with the Earth's geomagnetic field. According to *Tsurutani et al.* [1989], the southward interplanetary magnetic field is the most geoeffective parameter. While several studies have shown that the dawnside and nightside chorus respond quickly to southward interplanetary magnetic field, the exact time delay is not known. Therefore, time delays of up to 1440 min (24 h) at 30 min intervals were studied. In the following analysis  $B_s = -B_z$  is defined as the strength of the southward interplanetary magnetic field.  $B_s < 2$  nT is categorized as low,  $2 \text{ nT} < B_s < 4 \text{ nT}$  moderate, and  $B_s > 4 \text{ nT}$  high. Figure 8 shows the average lower band chorus intensities as a function of  $L$ , MLT, and  $B_s$  for low (left column), moderate (middle column), and high (right column)  $B_s$ . The results are shown for  $B_s$  with 60 ( $B_{s60}$ , top row), 90 ( $B_{s90}$ , middle row), and 120 ( $B_{s120}$ , bottom row) min of delay. Similar to solar wind velocity (Figure 2), the average chorus intensities increase with increasing  $B_s$ . The Kullback-Leibler theory was applied to calculate  $D_{KL}$ , between low and moderate ( $D_{KLlm}$ ), low and high ( $D_{KLlh}$ ), and moderate and high ( $D_{KLmh}$ )  $B_s$  for each particular cases of delay, as shown in Table 4. In this case, the only valid statistical distribution is observed with 90 min of delay in  $B_s$  ( $B_{s90}$ , middle row) with a  $D_{KLlh}$  value of 0.0766 (Note that the Kullback-Leibler results for delays of larger than 120 min provided invalid distributions and were increasingly more random).

**Table 4.** The Kullback-Leibler Distance ( $D_{KL}$ ) Between Low and Moderate ( $D_{KLlm}$ ), Low and High ( $D_{KLlh}$ ), and Moderate and High ( $D_{KLmh}$ )  $B_s$  for  $B_{s60}$ ,  $B_{s90}$ , and  $B_{s120}$  as Presented in Figure 8

	$D_{KLlm}$	$D_{KLmh}$	$D_{KLlh}$
$B_{s60}$	0.0328	0.0894	0.0825
$B_{s90}$	0.0393	0.0667	0.0766
$B_{s120}$	0.0339	0.0713	0.0631

Figure 9 shows the equatorial ( $|\lambda_m| < 15^\circ$ ) lower band (a), equatorial upper band (b), midlatitude ( $15^\circ \leq |\lambda_m| \leq 40^\circ$ ) lower band (c), and midlatitude upper band (d) average chorus intensities as a function of  $L$ , MLT, and  $B_s$  with 90 min of delay for low (left column), moderate (middle column), and high (right column)  $B_s$ . The results show significant similarities to solar wind velocity (Figure 3) and geomagnetic activity (Figure 1) with regards to the intensities of chorus emission. The average chorus intensities increase with increasing  $B_s$ . The average lower band chorus intensities are larger than the corresponding upper band chorus intensities. The upper band chorus intensities are mostly weak with peak values of less than 10 pT. The peak equatorial lower band chorus intensities are more widely distributed (from premidnight to early afternoon in the region of  $4 \leq L \leq 9$ ) compared to the midlatitude lower band chorus (from dawn to afternoon in the region of  $4 \leq L \leq 9$ ). Also, the peak lower band chorus intensities of 50 pT are more commonly observed with high  $B_s$  than with low solar wind density and high pressure. Overall, results indicate that the intensity

equatorial lower band chorus intensities are more widely distributed (from premidnight to early afternoon in the region of  $4 \leq L \leq 9$ ) compared to the midlatitude lower band chorus (from dawn to afternoon in the region of  $4 \leq L \leq 9$ ). Also, the peak lower band chorus intensities of 50 pT are more commonly observed with high  $B_s$  than with low solar wind density and high pressure. Overall, results indicate that the intensity

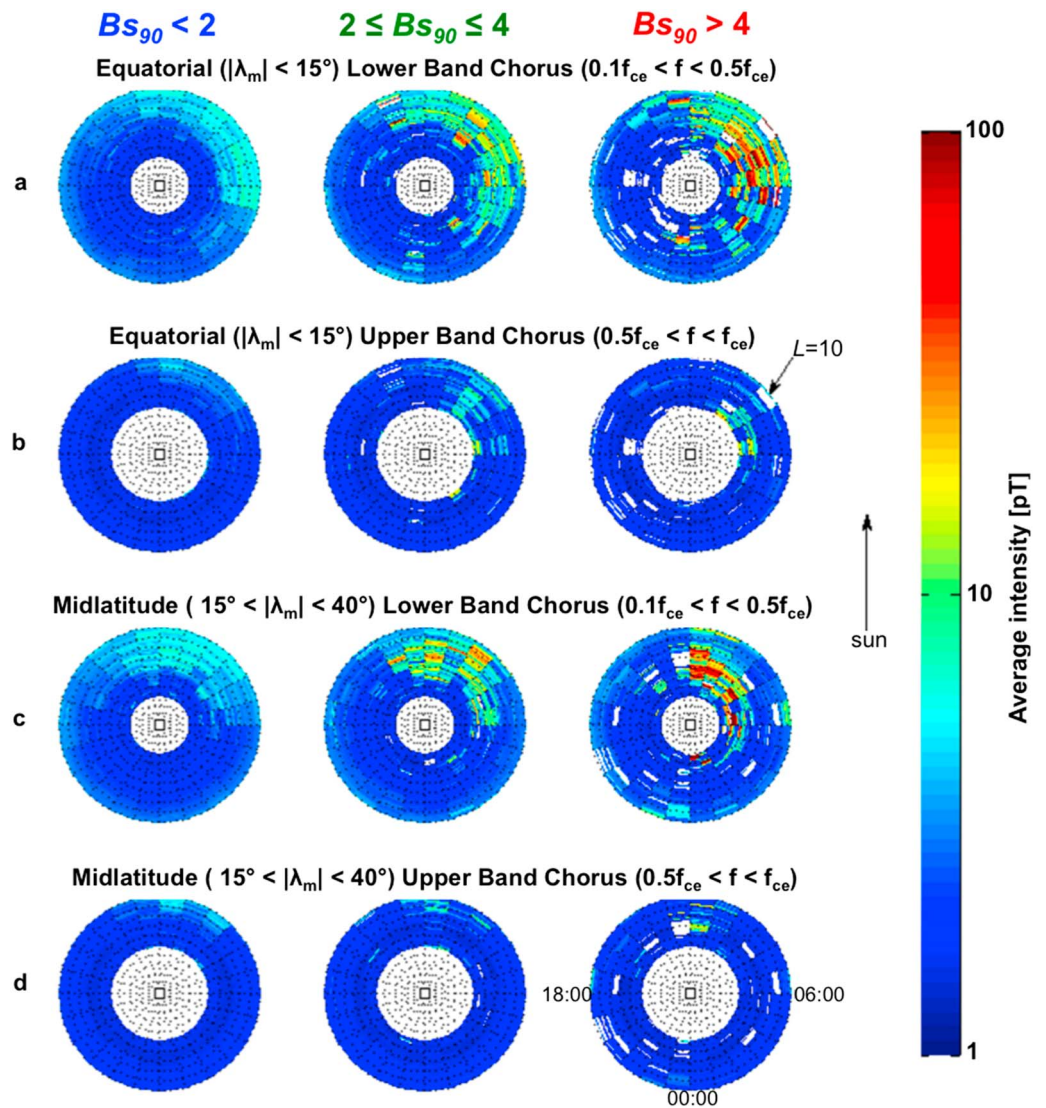


**Figure 9.** The (a) equatorial ( $|\lambda_m| < 15^\circ$ ) lower band, (b) equatorial upper band, midlatitude ( $15^\circ \leq |\lambda_m| \leq 40^\circ$ ), (c) lower band, and (d) midlatitude upper band average chorus intensities as a function of  $L$ , MLT, and ( $B_{z90}$ ) with 90 min of delay for (left column) low, (middle column) moderate, and (right column) high  $B_s$ .

of chorus emission is not only dependent on geomagnetic activity but also dependent on solar wind velocity, density, pressure, and vertical interplanetary magnetic field component.  $B_s$  and solar wind velocity are evidently the most influential parameters having the largest  $D_{KL}$  value between the extreme ends of the distributions ( $D_{KLih} = 0.0766$ ) and ( $D_{KLsf} = 0.0635$ ), respectively, followed by pressure ( $D_{KLih} = 0.0517$ ) and density ( $D_{KLih} = 0.0500$ ). The results here are in line with previous studies that have also identified solar wind velocity as highly influential solar wind parameter that control the flux of energetic electrons at geostationary orbit.

#### 4. Discussions and Conclusions

The present study examined almost 4 years (1 January 2004 to 29 September 2007) of STAFF (Spatio-Temporal Analysis of Field Fluctuation) data from Double Star TC1 and OMNI database. The results are largely comparable with previous studies that presented model wave distributions in the inner magnetosphere under different values of geomagnetic activity as expressed by the geomagnetic indices ( $Kp$  and  $Ae$ ) [Meredith *et al.*, 2003; Li *et al.*, 2011; Meredith *et al.*, 2012; Agapitov *et al.*, 2012, 2013]. In particular, the results here agree with the results of Meredith *et al.* [2012] who used the geomagnetic index,  $Ae$ , to study the distributions of the upper and lower band chorus intensities. However, in the present study the set of parameters of the wave distributions was expanded to include the solar wind parameters (velocity, density, pressure, and  $B_s$ ) in addition to the geomagnetic activity. The results strongly suggest that the intensity of chorus emission is not only dependent on geomagnetic activity but also dependent on solar wind parameters. The strong dependency between the intensity of chorus emission and the solar wind parameters shown here is not peculiar given the fact that various studies in the past [e.g., Snyder *et al.*, 1963; Gholipour *et al.*, 2004; Elliott *et al.*, 2013] identified a high correlation coefficient between geomagnetic indices and solar wind parameters.

Generally, the average upper band chorus intensities are relatively weak with peak values largely below 10 pT in all cases (chorus intensity as a function of geomagnetic activity, solar wind velocity, density, pressure, and  $B_s$ ). The largest intensities of the order 50 pT are observed for lower band chorus during active conditions, high solar wind velocities, low solar wind densities, high pressures, and high  $B_s$  correspondingly. Perhaps, the upper band chorus intensities are weaker than the lower band chorus because the generation of the upper band chorus requires higher anisotropy of resonant electrons [Kennel and Petschek, 1966]. It is known that electron injection and anisotropy depends upon geomagnetic activity and solar wind parameters. The resonant anisotropy and the resonant numbers of electrons largely determine the chorus wave instability [Xiao *et al.*, 1998, 2006]. The natural enhancement of electron anisotropy in the noon sector may result in high occurrence of dayside chorus at higher  $L$  [West *et al.*, 1973] where critical stably trapped flux levels are low. Electron injection would further enhance wave excitation [Li *et al.*, 2009]. This could account for the fact that chorus wave activities are associated with geomagnetic activity and also solar wind parameters.

The occurrence of peak lower band chorus intensities are most extensive during active conditions, fast solar wind velocities, and high  $B_s$  (from 2300 to 1300 MLT in the region of  $4 \leq L \leq 9$ ) but slightly less extensive during low solar wind densities and high pressures (from 0500 to 1200 MLT in the region of  $4 \leq L \leq 9$ ). The peak midlatitude ( $15^\circ \leq |\lambda_m| \leq 40^\circ$ ) chorus intensities predominantly occur within smaller MLT slots than the corresponding equatorial ( $|\lambda_m| < 15^\circ$ ) chorus intensities for both the upper and lower band chorus. Possibly, this is because Landau damping weakens some of the waves as they propagate to higher latitudes, where the wave normal angles are more oblique [Li *et al.*, 2010, 2011].

Evidently, the intensity of chorus emission is more dependent on solar wind velocity and  $B_s$  than solar wind density and pressure. Based on the Kullback-Leibler theory, the most widespread distribution was observed with  $B_s$  ( $D_{KLih} = 0.0766$ ) and solar wind velocity ( $D_{KLsf} = 0.0635$ ) followed by pressure ( $D_{KLih} = 0.0517$ ) and density ( $D_{KLih} = 0.0500$ ). This suggests that  $B_s$  and velocity are the most influential solar wind parameter that affect the evolution of the magnetospheric chorus wave intensities, consistent with the results of Kim *et al.* [2013] who presented an empirical model of the global distributions of the magnetospheric chorus amplitude using an artificial neural network and utilized the instantaneous measurement of the solar wind parameters as input. However, the present study takes into account the time delay introduced by the magnetospheric system. The results demonstrates that the most widespread statistical distributions are observed with a time delay of 90 min in  $B_z$  and a time delay of 1 day in solar wind velocity and density.

Studies of the evolution of energetic electron fluxes rely heavily on the numerical codes in order to model energy and pitch angle diffusion due to electron interaction with plasma waves in the frame of quasi-linear approximation. Therefore, including the solar wind parameters in addition to the geomagnetic activity in the statistical wave models will benefit those studies, provide a better representation of the wave distributions in the magnetosphere, and improve our knowledge of the acceleration and loss of radiation belt electrons.

#### Acknowledgments

Double Star was a joint mission by the European Space Agency (ESA) and the China National Space Administration. The STAFF and DWP experiments, operations, and data analysis were supported by CNES (France), STFC (UK), and ESA. The OMNI data were obtained from the GSFC/SPDF OMNI-Web interface at <http://omniweb.gsfc.nasa.gov>. H. Aryan would like to acknowledge financial support from EPSRC. The authors would like to thank the reviewers for their time and valuable comments.

Yuming Wang thanks the reviewers for their assistance in evaluating this paper.

#### References

- Agapitov, O., V. Krasnoselskikh, Y. V. Khotyaintsev, and G. Rolland (2012), Correction to: A statistical study of the propagation characteristics of whistler waves observed by Cluster, *Geophys. Res. Lett.*, *39*, L24102, doi:10.1029/2012GL054320.
- Agapitov, O., A. Artemyev, V. Krasnoselskikh, Y. V. Khotyaintsev, D. Mourenas, H. Breuillard, M. Balikhin, and G. Rolland (2013), Statistics of whistler mode waves in the outer radiation belt: Cluster STAFF-SA measurements, *J. Geophys. Res. Space Physics*, *118*, 3407–3420, doi:10.1002/jgra.50312.
- Artemyev, A. V., O. V. Agapitov, D. Mourenas, V. Krasnoselskikh, and L. M. Zelenyi (2013), Storm-induced energization of radiation belt electrons: Effect of wave obliquity, *Geophys. Res. Lett.*, *40*, 4138–4143, doi:10.1002/grl.50837.
- Aryan, H., R. J. Boynton, and S. N. Walker (2013), Analysis of trends between solar wind velocity and energetic electron fluxes at geostationary orbit using the reverse arrangement test, *J. Geophys. Res. Space Physics*, *118*, 636–641, doi:10.1029/2012JA018216.
- Baker, D. N., and S. G. Kanekal (2008), Solar cycle changes, geomagnetic variations, and energetic particle properties in the inner magnetosphere, *J. Atmos. Sol. Terr. Phys.*, *70*, 195–206, doi:10.1016/j.jastp.2007.08.031.
- Baker, D. N., J. B. Blake, L. B. Callis, J. R. Cummings, D. Hovestadt, S. Kanekal, B. Klecker, R. A. Mewaldt, and R. D. Zwickl (1994), Relativistic electron acceleration and decay time scales in the inner and outer radiation belts: SAMPEX, *Geophys. Res. Lett.*, *21*(6), 409–412, doi:10.1029/93GL03532.
- Baker, D. N., et al. (2014), Gradual diffusion and punctuated phase space density enhancements of highly relativistic electrons: Van Allen Probes observations, *Geophys. Res. Lett.*, *41*, 1351–1358, doi:10.1002/2013GL058942.
- Balikhin, M. A., R. J. Boynton, S. A. Billings, M. Gedalin, N. Ganushkina, D. Coca, and H. Wei (2010), Data based quest for solar wind-magnetosphere coupling function, *Geophys. Res. Lett.*, *37*, L24107, doi:10.1029/2010GL045733.
- Balikhin, M. A., R. J. Boynton, S. Walker, J. E. Borovsky, S. A. Billings, and H. L. Wei (2011), Using the NARMAX approach to model the evolution of energetic electrons fluxes at geostationary orbit, *Geophys. Res. Lett.*, *38*, L18105, doi:10.1029/2011GL048980.
- Blake, J. B., M. S. Gussenhoven, E. G. Mullen, and R. W. Fillius (1992), Identification of an unexpected space radiation hazard, *IEEE Trans. Nucl. Sci.*, *39*, 1761–1764, doi:10.1109/23.211364.
- Bortnik, J., and R. M. Thorne (2007), The dual role of ELF/VLF chorus waves in the acceleration and precipitation of radiation belt electrons, *J. Atmos. Sol. Terr. Phys.*, *69*, 378–386, doi:10.1016/j.jastp.2006.05.030.
- Bortnik, J., W. Li, R. M. Thorne, V. Angelopoulos, C. Cully, J. Bonnell, O. Le Contel, and A. Roux (2009), An observation linking the origin of plasmaspheric hiss to discrete chorus emissions, *Science*, *324*, 775–778, doi:10.1126/science.1171273.
- Boynton, R. J., M. A. Balikhin, S. A. Billings, H. L. Wei, and N. Ganushkina (2011), Using the NARMAX OLS-ERR algorithm to obtain the most influential coupling functions that affect the evolution of the magnetosphere, *J. Geophys. Res.*, *116*, A05218, doi:10.1029/2010JA015505.
- Boynton, R. J., M. A. Balikhin, S. A. Billings, G. D. Reeves, N. Ganushkina, M. Gedalin, O. A. Amariutei, J. E. Borovsky, and S. N. Walker (2013), The analysis of electron fluxes at geosynchronous orbit employing a NARMAX approach, *J. Geophys. Res. Space Physics*, *118*, 1500–1513, doi:10.1002/jgra.50192.
- Burtis, W. J., and R. A. Helliwell (1969), Banded chorus—A new type of VLF radiation observed in the magnetosphere by OGO 1 and OGO 3, *J. Geophys. Res.*, *74*, 3002–3010, doi:10.1029/JA074i011p03002.
- Cornilleau-Wehrin, N., et al. (2005), The STAFF-DWP wave instrument on the DSP equatorial spacecraft: Description and first results, *Ann. Geophys.*, *23*, 2785–2801, doi:10.5194/angeo-23-2785-2005.
- Craven, J. D. (1966), Temporal variations of electron intensities at low altitudes in the outer radiation zone as observed with satellite Injun 3, *J. Geophys. Res.*, *71*, 5643–5663, doi:10.1029/JZ071i023p05643.
- Elliott, H. A., J.-M. Jahn, and D. J. McComas (2013), The Kp index and solar wind speed relationship: Insights for improving space weather forecasts, *Space Weather*, *11*, 339–349, doi:10.1002/swe.20053.
- Fennell, J. F., H. C. Koons, J. L. Roeder, and J. B. Blake (2001), Spacecraft charging: Observations and relationship to satellite anomalies, in *Spacecraft Charging Technology*, ESA Special Publication, vol. 476, edited by R. A. Harris, 279 pp., European Space Agency, ESA, Noordwijk, Netherlands.
- Gholipour, A., C. Lucas, and B. N. Araabi (2004), Black box modeling of magnetospheric dynamics to forecast geomagnetic activity, *Space Weather*, *2*, S07001, doi:10.1029/2003SW000039.
- Helliwell, R. A. (1967), A theory of discrete VLF emissions from the magnetosphere, *J. Geophys. Res.*, *72*, 4773–4790, doi:10.1029/JZ072i019p04773.
- Kennel, C. F., and H. E. Petschek (1966), Limit on stably trapped particle fluxes, *J. Geophys. Res.*, *71*, 1–28.
- Kim, K.-C., Y. Shprits, J. Lee, and J. Hwang (2013), Empirically modeled global distribution of magnetospheric chorus amplitude using an artificial neural network, *J. Geophys. Res. Space Physics*, *118*, 6243–6253, doi:10.1002/jgra.50595.
- Kullback, S. (1959), Information theory and statistics, in *Information Theory and Statistics*, Wiley Series in Probability and Mathematical Statistics, pp. 1–256, John Wiley, New York.
- Kullback, S., and R. A. Leibler (1951), On information and sufficiency, *Ann. Math. Stat.*, *22*, 79–86, doi:10.1214/aoms/1177729694.
- Lauben, D. S., U. S. Inan, T. F. Bell, and D. A. Gurnett (2002), Source characteristics of ELF/VLF chorus, *J. Geophys. Res.*, *107*(A12), 1429, doi:10.1029/2000JA003019.
- LeDocq, M. J., D. A. Gurnett, and G. B. Hospodarsky (1998), Chorus source locations from VLF Poynting flux measurements with the Polar spacecraft, *Geophys. Res. Lett.*, *25*, 4063–4066, doi:10.1029/1998GL900071.
- Li, W., Y. Y. Shprits, and R. M. Thorne (2007), Dynamic evolution of energetic outer zone electrons due to wave-particle interactions during storms, *J. Geophys. Res.*, *112*, A10220, doi:10.1029/2007JA012368.
- Li, W., R. M. Thorne, V. Angelopoulos, J. Bortnik, C. M. Cully, Ni. B., O. Le Contel, A. Roux, U. Auster, and W. Magnes (2009), Global distribution of whistler-mode chorus waves observed on the THEMIS spacecraft, *Geophys. Res. Lett.*, *36*, L09104, doi:10.1029/2009GL037595.

- Li, W., et al. (2010), THEMIS analysis of observed equatorial electron distributions responsible for the chorus excitation, *J. Geophys. Res.*, *115*, A00F11, doi:10.1029/2009JA014845.
- Li, W., J. Bortnik, R. M. Thorne, and V. Angelopoulos (2011), Global distribution of wave amplitudes and wave normal angles of chorus waves using THEMIS wave observations, *J. Geophys. Res.*, *116*, A12205, doi:10.1029/2011JA017035.
- Li, X., D. N. Baker, M. Teremin, T. E. Cayton, G. D. Reeves, R. S. Selesnick, J. B. Blake, G. Lu, S. G. Kanekal, and H. J. Singer (1999), Rapid enhancements of relativistic electrons deep in the magnetosphere during the May 15, 1997, magnetic storm, *J. Geophys. Res.*, *104*, 4467–4476, doi:10.1029/1998JA900092.
- Li, X., D. N. Baker, M. Temerin, G. Reeves, R. Friedel, and C. Shen (2005), Energetic electrons, 50 keV to 6 MeV, at geosynchronous orbit: Their responses to solar wind variations, *Space Weather*, *3*, S04001, doi:10.1029/2004SW000105.
- Lyons, L. R., R. M. Thorne, and C. F. Kennel (1972), Pitch-angle diffusion of radiation belt electrons within the plasmasphere, *J. Geophys. Res.*, *77*, 3455–3474, doi:10.1029/JA077i019p03455.
- Matsumura, C., Y. Miyoshi, K. Seki, S. Saito, V. Angelopoulos, and J. Koller (2011), Outer radiation belt boundary location relative to the magnetopause: Implications for magnetopause shadowing, *J. Geophys. Res.*, *116*, A06212, doi:10.1029/2011JA016575.
- Meredith, N. P., R. B. Horne, R. H. A. Iles, R. M. Thorne, D. Heynderickx, and R. R. Anderson (2002), Outer zone relativistic electron acceleration associated with substorm-enhanced whistler mode chorus, *J. Geophys. Res.*, *107*(A7), 0148–0227, doi:10.1029/2001JA900146.
- Meredith, N. P., R. B. Horne, R. M. Thorne, and R. R. Anderson (2003), Favored regions for chorus-driven electron acceleration to relativistic energies in the Earth's outer radiation belt, *Geophys. Res. Lett.*, *30*(16), 1871, doi:10.1029/2003GL017698.
- Meredith, N. P., R. B. Horne, A. Sicard-Piet, D. Boscher, K. H. Yearby, W. Li, and R. M. Thorne (2012), Global model of lower band and upper band chorus from multiple satellite observations, *J. Geophys. Res.*, *117*, A10225, doi:10.1029/2012JA017978.
- Millan, R. M., and R. M. Thorne (2007), Review of radiation belt relativistic electron losses, *J. Atmos. Sol. Terr. Phys.*, *69*, 362–377, doi:10.1016/j.jastp.2006.06.019.
- Mourenas, D., A. V. Artemyev, O. V. Agapitov, and V. Krasnoselskikh (2013), Analytical estimates of electron quasi-linear diffusion by fast magnetosonic waves, *J. Geophys. Res. Space Physics*, *118*, 3096–3112, doi:10.1002/jgra.50349.
- Ohtani, S., Y. Miyoshi, H. J. Singer, and J. M. Weygand (2009), On the loss of relativistic electrons at geosynchronous altitude: Its dependence on magnetic configurations and external conditions, *J. Geophys. Res.*, *114*, A01202, doi:10.1029/2008JA013391.
- Onsager, T. G., J. C. Green, G. D. Reeves, and H. J. Singer (2007), Solar wind and magnetospheric conditions leading to the abrupt loss of outer radiation belt electrons, *J. Geophys. Res.*, *112*, A01202, doi:10.1029/2006JA011708.
- Paulikas, G. A., and J. B. Blake (1979), Effects of the solar wind on magnetospheric dynamics—Energetic electrons at the synchronous orbit, in *Quantitative Modeling of Magnetospheric Processes*, *Geophys. Monogr. Ser.*, edited by W. P. Olson, pp. 180–202, AGU, Washington, D. C.
- Reeves, G. D., K. L. McAdams, R. H. W. Friedel, and T. P. O'Brien (2003), Acceleration and loss of relativistic electrons during geomagnetic storms, *Geophys. Res. Lett.*, *30*(10), 1529, doi:10.1029/2002GL016513.
- Reeves, G. D., S. K. Morley, R. H. W. Friedel, M. G. Henderson, T. E. Cayton, G. Cunningham, J. B. Blake, R. A. Christensen, and D. Thomsen (2011), On the relationship between relativistic electron flux and solar wind velocity, *J. Geophys. Res.*, *116*, A02213, doi:10.1029/2010JA015735.
- Reeves, G. D., S. Morley, and G. Cunningham (2013), Long-term variations in solar wind velocity and radiation belt electrons, *J. Geophys. Res. Space Physics*, *118*, 1040–1048, doi:10.1002/jgra.50126.
- Santolík, O., E. Macušová, K. H. Yearby, N. Cornilleau-Wehrlin, and H. S. K. Alleyne (2005), Radial variation of whistler-mode chorus: First results from the STAFF/DWP instrument on board the Double Star TC-1 spacecraft, *Ann. Geophys.*, *23*, 2937–2942, doi:10.5194/angeo-23-2937-2005.
- Shprits, Y. Y., D. Subbotin, and B. Ni (2009), Evolution of electron fluxes in the outer radiation belt computed with the VERB code, *J. Geophys. Res.*, *114*, A11209, doi:10.1029/2008JA013784.
- Snyder, C. W., M. Neugebauer, and U. R. Rao (1963), The solar wind velocity and its correlation with cosmic-ray variations and with solar and geomagnetic activity, *J. Geophys. Res.*, *68*(24), 6361–6370, doi:10.1029/JZ068i024p06361.
- Summers, D., B. Ni, and N. P. Meredith (2007), Timescales for radiation belt electron acceleration and loss due to resonant wave-particle interactions: 2. Evaluation for VLF chorus, ELF hiss, and electromagnetic ion cyclotron waves, *J. Geophys. Res.*, *112*, A04207, doi:10.1029/2006JA011993.
- Thorne, R. M., T. P. O'Brien, Y. Y. Shprits, D. Summers, and R. B. Horne (2005), Timescale for MeV electron microburst loss during geomagnetic storms, *J. Geophys. Res.*, *110*, A09202, doi:10.1029/2004JA010882.
- Thorne, R. M., et al. (2013), Rapid local acceleration of relativistic radiation-belt electrons by magnetospheric chorus, *Nature*, *504*, 411–414, doi:10.1038/nature12889.
- Tsurutani, B. T., and E. J. Smith (1974), Postmidnight chorus: A substorm phenomenon, *J. Geophys. Res.*, *79*, 118–127, doi:10.1029/JA079i001p00118.
- Tsurutani, B. T., A. L. Brinca, E. J. Smith, R. T. Okida, and R. R. Anderson (1989), A statistical study of ELF-VLF plasma waves at the magnetopause, *J. Geophys. Res.*, *94*, 1270–1280, doi:10.1029/JA094iA02p01270.
- Tu, W., X. Li, Y. Chen, G. D. Reeves, and M. Temerin (2009), Storm-dependent radiation belt electron dynamics, *J. Geophys. Res.*, *114*, 0148–0227, doi:10.1029/2008JA013480.
- West, H. I., R. M. Buck, and J. R. Walton (1973), Electron pitch angle distributions throughout the magnetosphere as observed on Ogo 5, *J. Geophys. Res.*, *78*(7), 1064–1081, doi:10.1029/JA078i007p01064.
- Xiao, F., R. M. Thorne, and D. Summers (1998), Instability of electromagnetic R-mode waves in a relativistic plasma, *Phys. Plasmas*, *5*, 2489–2497, doi:10.1063/1.872932.
- Xiao, F., Q. Zhou, H. He, and L. Tang (2006), Instability of whistler-mode waves by a relativistic kappa-loss-cone distribution in space plasmas, *Plasma Phys. Controlled Fusion*, *48*, 1437–1445, doi:10.1088/0741-3335/48/9/012.
- Xiao, F., Z. Su, H. Zheng, and S. Wang (2009), Modeling of outer radiation belt electrons by multidimensional diffusion process, *J. Geophys. Res.*, *114*, A03201, doi:10.1029/2008JA013580.
- Xiao, F., Z. Su, H. Zheng, and S. Wang (2010), Three-dimensional simulations of outer radiation belt electron dynamics including cross-diffusion terms, *J. Geophys. Res.*, *115*, A05216, doi:10.1029/2009JA014541.